A FULLY COUPLED MULTISCALE SHELL FORMULATION FOR THE MODELLING OF FIBRE REINFORCED LAMINATES

J. Främby*[1], J. Brouzoulis[1], M. Fagerström[1], R. Larsson[1]

[1] *Department of Applied Mechanics, Chalmers University of Technology, Gothenburg, Sweden*
* *Corresponding Author: johannes.framby@chalmers.se*

Keywords: multiscale, FRP, laminate, through-thickness stress distribution,

Abstract
In this contribution, we discuss the potential of using a fully coupled multiscale method based on computational homogenisation for simulating the mechanical response of fibre reinforced thin-walled laminates based on shell theory. Emphasis is placed on the effect of e.g. RVE size on the results as compared to both a fully resolved 3D analysis and a pure shell analysis. In the investigations of the method, we restrict to elastic response and focus on the pros and cons of the approach in terms of the accuracy in the through-thickness direction and the benefits thereof in predicting onset of e.g. matrix and/or delamination cracks. It is clear that with the adopted boundary conditions, the 'best' results (in terms of stress distribution compared to the reference case in 3D) that can be achieved corresponds to what is obtained in the shell analysis.

1. Introduction

Numerical tools for the accurate prediction of crash response in lightweight designed vehicle structures using FRP:s are crucial for structural composites to have a widespread use in future cars. Consequently, for an accurate prediction of the crashworthiness performance, careful account of the dominating failure mechanisms are necessary for the proper modelling of progressive laminate failure in this type of application. In an attempt to meet this goal, we introduce a multiscale method based on shell theory for simulation of the mechanical response of fibre reinforced thin-walled laminates. The main idea is to use a nested computational multiscale analysis, *cf.* Figure 1, while still allowing for shell modelling of the macroscale, in order to reduce the computational cost, as discussed by Larsson and Landervik [1]. In the current method, the momentum balance is set up as an initial boundary value problem on the macroscale, where the laminate level is explicitly accounted for via nested FE analyses of Representative Volume Elements (RVE:s), *cf.* Kouznetsova *et al.* [2], providing the homogenised stress resultants in each integration point of the shell surface. In the present investigation, we restrict the numerical investigations to elastic behaviour and focus on the pros and cons of the approach in terms of the accuracy in the through-thickness variation of out-of-plane stress components which for traditional shell formulations is rather low. A related investigation in this context has been carried out by Hosseini *et al.* [3] providing good estimates of the out-of-plane components for isogeometric shell analyses. We emphasise that our approach is quite general and it may well be applied to the modelling of local non-linear effects such as local damage progression at the ply level, *cf.* Coenen *et al.* [4].

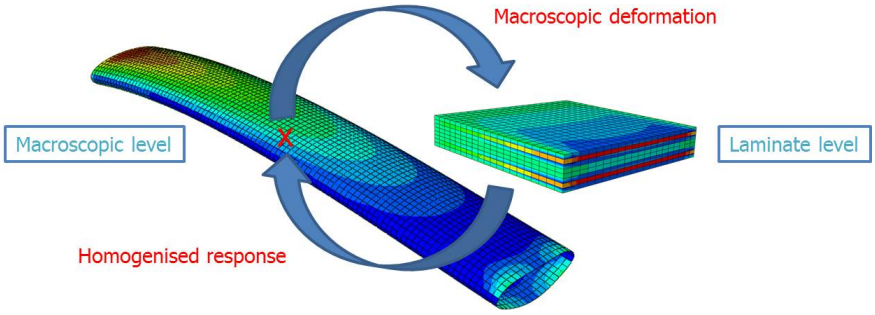

Figure 1. Figure showing the principles of the multiscale approach.

2. Macroscopic kinematics

2.1. Initial shell geometry and convected coordinates

As a staring point, the initial configuration B_0 of the shell is considered parametrised in terms of convected (covariant) coordinates (ξ_1, ξ_2, ξ) as

$$\mathrm{B}_0 = \left\{ \boldsymbol{X} := \boldsymbol{\Phi}(\boldsymbol{\xi}) = \boldsymbol{\Phi}_0(\boldsymbol{\xi}_0) + \xi \boldsymbol{M}(\boldsymbol{\xi}_0) \text{ with } \boldsymbol{\xi}_0 \in A \text{ and } \xi \in \frac{h_0}{2}[-1,1] \right\} \tag{1}$$

where we introduced the compact notation $\boldsymbol{\xi} = (\xi_1, \xi_2, \xi)$ and $\boldsymbol{\xi}_0 = (\xi_1, \xi_2)$ and where the mapping $\boldsymbol{\Phi}(\boldsymbol{\xi})$ maps the inertial Cartesian frame into the undeformed configuration, *cf.* Figure 2. In Eq. (1), the mapping $\boldsymbol{\Phi}$ is defined by the midsurface placement $\boldsymbol{\Phi}_0$ and the outward unit normal vector field $\boldsymbol{M}$ (with $|\boldsymbol{M}| = 1$). The coordinate ξ is associated with this direction and h_0 is the initial thickness of the shell. Furthermore, it should be noted that

$$\mathrm{d}\boldsymbol{X} = (\boldsymbol{G}_\alpha \otimes \boldsymbol{G}^\alpha) \cdot \mathrm{d}\boldsymbol{X} + \boldsymbol{M} \otimes \boldsymbol{M} \cdot \mathrm{d}\boldsymbol{X} = \boldsymbol{G}_\alpha(\boldsymbol{\xi})\mathrm{d}\xi_\alpha + \boldsymbol{M}(\boldsymbol{\xi}_0)\mathrm{d}\xi \tag{2}$$

whereby the covariant basis vectors are defined by $\{\boldsymbol{G}_\alpha = \boldsymbol{\Phi}_{0,\alpha} + \xi \boldsymbol{M}_{,\alpha}\}_{\alpha=1,2}$ and $\boldsymbol{G}_3 = \boldsymbol{G}^3 = \boldsymbol{M}$, where $\bullet_{,\alpha}$ denotes the derivative with respect to ξ_α.

2.2. Current shell geometry

The current (deformed) geometry is in the present formulation described by the deformation map $\boldsymbol{\varphi}(\boldsymbol{\xi}) \in \mathcal{B}$ of the inertial Cartesian frame as

$$\boldsymbol{x}(\boldsymbol{\xi}) = \boldsymbol{\varphi}(\boldsymbol{\xi}) = \boldsymbol{\varphi}_0(\boldsymbol{\xi}_0) + \xi \boldsymbol{m}(\boldsymbol{\xi}_0) + \frac{1}{2}\xi^2 \gamma(\boldsymbol{\xi}_0)\boldsymbol{m}(\boldsymbol{\xi}_0) \tag{3}$$

where the mapping is defined by the midsurface placement $\boldsymbol{\varphi}_0$, the spatial director field $\boldsymbol{m}$ and an additional scalar thickness inhomogeneity strain γ, *cf.* also Figure 2. As can be seen, the specification of the current configuration corresponds to a second order Taylor expansion along the director field, involving the inhomogeneity strain γ, thereby describing inhomogeneous thickness deformation effects of the shell. In particular, the pathological Poisson locking effect is avoided in this fashion. The pertinent deformation gradient $\boldsymbol{F}$ to the adopted kinematics is defined as

$$\mathrm{d}\boldsymbol{x} = \boldsymbol{F} \cdot \mathrm{d}\boldsymbol{X} \text{ with } \boldsymbol{F} = \boldsymbol{g}_i \otimes \boldsymbol{G}^i, \quad i = 1,2,3 \tag{4}$$

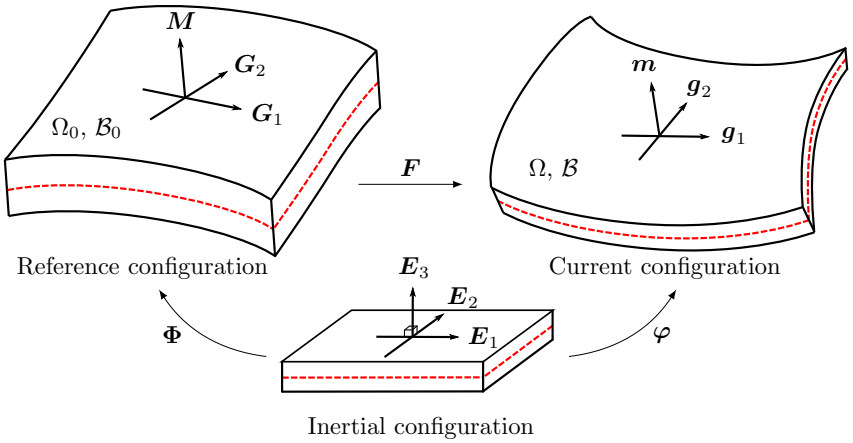

Figure 2. Mappings of shell model defining undeformed and deformed shell configurations relative to inertial Cartesian frame.

where, as shown in Reference [1], the spatial covariant basis vectors are given as

$$\boldsymbol{g}_\alpha = \boldsymbol{\varphi}_{0,\alpha} + \left(\xi + \frac{1}{2}\gamma\xi^2\right)\boldsymbol{m}_{,\alpha} + \frac{1}{2}\gamma_{,\alpha}\xi^2\boldsymbol{m},\ \alpha = 1,2;\ \boldsymbol{g}_3 = (1+\gamma\xi)\,\boldsymbol{m} \tag{5}$$

This kinematic representation is then inserted in the (static) momentum balance between internal and external forces to obtain the resulting shell element formulation, *cf.* Larsson and Landervik for details [1].

3. Laminate level kinematics for a representative volume element

Since the ambition is to establish a multiscale framework, we need to couple the above described macroscopic kinematical shell representation to a 3D resolution of the displacement field on the laminate level in the RVE. Following Larsson and Landervik [1], a key issue in the developments relates to the adopted shell kinematics, where it is assumed that the averaged deformation field varies slowly enough within the RVE to justify that it is *constant* in the *tangent* plane (=) directions of the shell. In the thickness ($\perp$) direction separation of micro- and macro scales cannot be assumed, whereby the microscopic fluctuations on the laminate level must be completely resolved in the $\perp$–direction. As to the the size of the RVE, we note that its thickness is given by the thickness of the thin–walled structure, whereas the in-plane breadth and width of the RVE should be chosen based on a balance between accuracy and computational efficiency as exemplified later in the numerical section. In the following, we consider quantities related to the macroscopic fields denoted by a superimposed bar, *e.g.* $\overline{\bullet}$.

3.1. Kinematic expansions of macroscopic fields in the RVE

In order to couple the macroscopic and the microscopic fields, different Taylor series expansions of the deformation map with respect to the RVE are made according to the tangent plane and thickness directions of the shell. Hence, the finite microscopic placement $\Delta\boldsymbol{x}[\boldsymbol{X}]$ (measured as the placement relative to the expansion point $\overline{\boldsymbol{X}}$) within the RVE is expressed in separate portions in the tangent- and the thickness directions, denoted by $\Delta\overline{\boldsymbol{x}}_=$ and $\Delta\overline{\boldsymbol{x}}_\perp$, respectively, *cf.* also Figure 3. Hence, together with the laminate level displacement field $\boldsymbol{u}_\mathrm{f}$, the relative

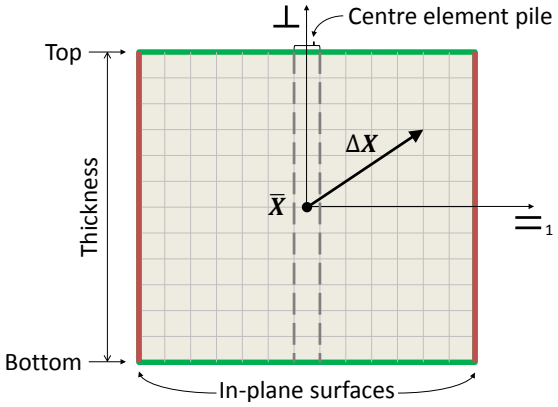

Figure 3. Sketch of midsection through the 12x13x13 (hexahedra) element RVE showing the expansion point $\overline{\boldsymbol{X}}$ and the placement vector $\Delta\boldsymbol{X}$ in the reference configuration. The thickness of the RVE is given by the plate thickness while the in-plane dimension is examined in Section 4.

placement $\Delta\boldsymbol{x}[\boldsymbol{X}]$ is expressed as

$$\Delta\boldsymbol{x} = \Delta\overline{\boldsymbol{x}}_{=} + \Delta\overline{\boldsymbol{x}}_{\perp} + \boldsymbol{u}_{\mathrm{f}} \tag{6}$$

where $\Delta\overline{\boldsymbol{x}}_{=}$ is defined by the first order expansion, at each level ξ in the ξ^{α} directions, of the RVE defined as

$$\Delta\overline{\boldsymbol{x}}_{=} = \overline{\boldsymbol{F}} \cdot \Delta\boldsymbol{X}_{=} = \overline{\boldsymbol{g}}_{\alpha|\xi}\Delta\xi^{\alpha} \text{ with } \Delta\boldsymbol{X}_{=} = \overline{\boldsymbol{G}}_{\alpha}\Delta\xi^{\alpha} \tag{7}$$

where the notation $\overline{\boldsymbol{g}}_{\alpha|\xi}$ implies that the expansion is made for a fixed value of ξ. The placement in the thickness direction $\Delta\overline{\boldsymbol{x}}_{\perp}$ is formulated as the second-order Taylor series expansion (involving the second gradient $\overline{\boldsymbol{K}} = (\overline{\boldsymbol{g}}_i \otimes \overline{\boldsymbol{G}}^i)_{,j} \otimes \overline{\boldsymbol{G}}^j$) about the *origin* of the RVE as

$$\Delta\overline{\boldsymbol{x}}_{\perp} = \overline{\boldsymbol{F}}_{|\xi=0} \cdot \Delta\boldsymbol{X}_{\perp} + \frac{1}{2}\left(\overline{\boldsymbol{K}}_{|\xi=0} \cdot \Delta\boldsymbol{X}_{\perp}\right) \cdot \Delta\boldsymbol{X}_{\perp} = \overline{\boldsymbol{g}}_{3|\xi=0}\xi + \frac{1}{2}\overline{\boldsymbol{g}}_{3,3|\xi=0}\xi^2 \tag{8}$$

Hence, in view of the relations (6)-(8), the kinematics of the RVE is obtained in terms of the generalised shell strain measures as

$$\Delta\boldsymbol{x} = \overline{\boldsymbol{g}}_{\alpha|\xi}\Delta\xi^{\alpha} + \overline{\boldsymbol{m}}(\xi + \frac{1}{2}\overline{\gamma}(\xi)^2) + \boldsymbol{u}_{\mathrm{f}}[\boldsymbol{X}] \tag{9}$$

and the deformation gradient $\mathrm{d}\Delta\boldsymbol{x} = \boldsymbol{F}\cdot\mathrm{d}\boldsymbol{X}$ on the laminate level associated with this kinematical description, with due consideration to that ξ is considered fixed in the expansion in (7), now finally becomes

$$\boldsymbol{F} = \left(\overline{\boldsymbol{g}}_i + \frac{\partial\boldsymbol{u}_f}{\partial\xi^i}\right) \otimes \overline{\boldsymbol{G}}^i = \overline{\boldsymbol{F}} + \boldsymbol{H}_f \text{ with } \overline{\boldsymbol{F}} = \overline{\boldsymbol{g}}_i \otimes \overline{\boldsymbol{G}}^i \text{ and } \boldsymbol{H}_f = \frac{\partial\boldsymbol{u}_{\mathrm{f}}}{\partial\boldsymbol{X}} \tag{10}$$

For further details about the associated homogenisation procedure interested readers are referred to [1]. Emphasis in the current contribution is instead put on assessing the potential of this method for obtaining accurate stress distributions in the laminate by means of multiscale modelling. For this purpose, we focus only on the prolongation conditions, *i.e.* the link from the macroscale shell problem to the laminate level RVE analysis and study the effect of the size and boundary conditions of the RVE.

3.2. Application of boundary conditions

The boundary conditions for the RVE analysis need to be chosen with due consideration to the adopted homogenisation procedure. Without going into details here, we follow Larsson and Landervik [1] and choose to apply Dirichlet boundary conditions on the in-plane surfaces of the RVE, *i.e.* prescribing the fluctuation field $\mathbf{u}_\mathrm{f}$ to vanish on these surfaces, whereas we apply Neumann (traction free) boundary conditions on the top and bottom surface, *cf.* Figure 3. This will in the sequel be denoted as the *Mixed* boundary conditions. What we want to investigate is if this choice of boundary conditions leads to an improved prediction of the distribution of the different stress components, compared to the more restricted shell theory case.

For comparison, we will also investigate a pure Dirichlet case, denoted *Dirichlet* boundary conditions in the sequel, with all six surfaces of the RVE subject to the condition that $\mathbf{u}_\mathrm{f} = \mathbf{0}$. This is a more restricted case and the assumption is that this choice of boundary conditions will yield a solution much closer to what is obtained from a pure shell analysis. As a final comparison, we will also investigate the response obtained for a Taylor assumption, *i.e.* the case where the fluctuation field $\mathbf{u}_\mathrm{f}$ is set to zero in the entire domain (*Taylor* boundary conditions).

4. Numerical results

Whether the multiscale approach yields a better approximation of the out-of-plane stress components was analysed in the numerical example below. A square plate, rigidly attached on one edge and subjected to a prescribed displacement of $\delta = 0.1$ mm on the opposite edge, has been simulated based both the proposed shell model and a 3D continuum solid model using a hexahedron element mesh, *cf.* Figure 4. The shell model consists of 450 isosceles right second order triangles (4 mm mesh size) and the solid model of 691200 linear square hexahedra (0.25 mm mesh size giving 12 element through the thickness). The RVE is modelled with the same square hexahedron element as in the solid plate, with 12 elements through the plate thickness. The in plane dimensions have been varied from 1.25 mm (5 elements) to 6.25 mm (25 elements). Small deformations are assumed.

To compare the results from the different models a shell integration point close to the middle of the plate is chosen. From this point the generalised strains of the shell model are extracted, *i.e.* $\overline{\boldsymbol{g}}_{\alpha|\xi}$, $\overline{\boldsymbol{m}}$ and $\overline{\gamma}$, so that the proper boundary displacement can be computed and applied to the RVE via Eq. (9); the through-thickness stress components were also extracted. At the same point in the solid model a vertical pile of elements is chosen, from which the average stress components of the four in-plane integration points are extracted at each $\perp$-level. Two approaches to extract the stress profiles from the deformed RVE have been studied: *i*) the in-plane integration point average of the centre element pile (*i.e* same method as in the solid plate model), *cf.* Figure 3, and *ii*) the in-plane average of all element integration points.

4.1. Isotropic cantilever beam

A first comparison of the stress components in the shell, the mult-scale and the solid models was made using an isotropic material with a Young's modulus of 70.7 GPa and a Poisson's ratio of zero. This allows for comparison to Euler-Bernoulli beam theory, to which the solid model, although piecewise linear in σ_{xz}, compares very well, *cf.* Figure 5a and 5e.

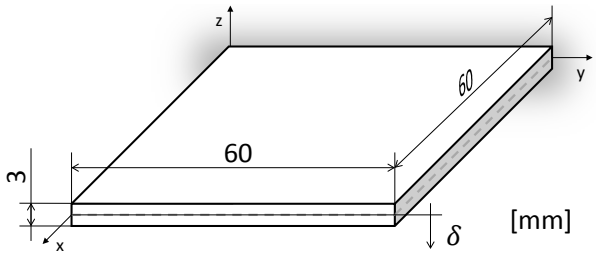

Figure 4. Sketch of the numerical example. *NB:* proportions not representative.

In Figure 5 the stress components from the different models with the first RVE extraction approach (in-plane integration point average in the centre element pile) is presented. In this comparison the *Mixed* boundary conditions have been applied on the RVE. The in-plane stress components σ_{xx} and σ_{yy} are similar in the shell and the solid models while increasing RVE-sizes diverge from these. However, all other stress components show differences between the models. Obviously an increasing RVE size does not converge towards the solid reference model, even though the profile shape of the σ_{xz}-component in the RVE show improvements w.r.t. the beam theory as the size increases. On the other hand smaller RVE sizes do converge towards the shell results. Please note that this also applies to higher mesh resolutions of the smallest RVE. These results imply that as the size of the RVE increases the applied deformation mode on the RVE becomes more inaccurate compared to both the reference shell and solid models.

Figure 6 shows that the second stress extraction approach (surface average of all integration points) on the RVE converge faster towards the shell results for decreasing size compared to only extracting the stress components of the centre elements. These results also show that the resulting shear force on the RVE decrease as the the RVE size increase.

The effect from applying different boundary conditions on the RVE, as stated in Section 3.2, is presented in Figure 7, where the 12x13x13 element sized RVE is taken as example. When the *Dirichlet* or the *Taylor* boundary conditions are applied the results in the RVE match the shell results rather well, which would be expected with the proposed shell kinematics.

4.2. Laminated cantilever beam

The simulation presented above has also been performed with the plate modelled as a $[\pm 45^\circ]_{3S}$ laminate of transverse isotropic laminae, having the material properties given in Table 1. In Figure 8 three stress components are compared for the shell and the solid models along with three RVE sizes (*Mixed* boundary conditions and centre element pile stress extraction). Neither the shell or any of the RVE:s can capture in-plane stress components of the solid model exactly, however, the variation of the out-of-plane shear stress in the largest RVE seems improved compared to the shell. As for the isotropic case smaller RVE sizes converge towards the shell results.

E_L [GPa]	E_T [GPa]	ν_{LT}	$\nu_{TT'}$	G_{LT} [GPa]	$G_{TT'}$ [GPa]
100	10	0.25	0.25	5.0	4.0

Table 1. Material properties for laminate model.

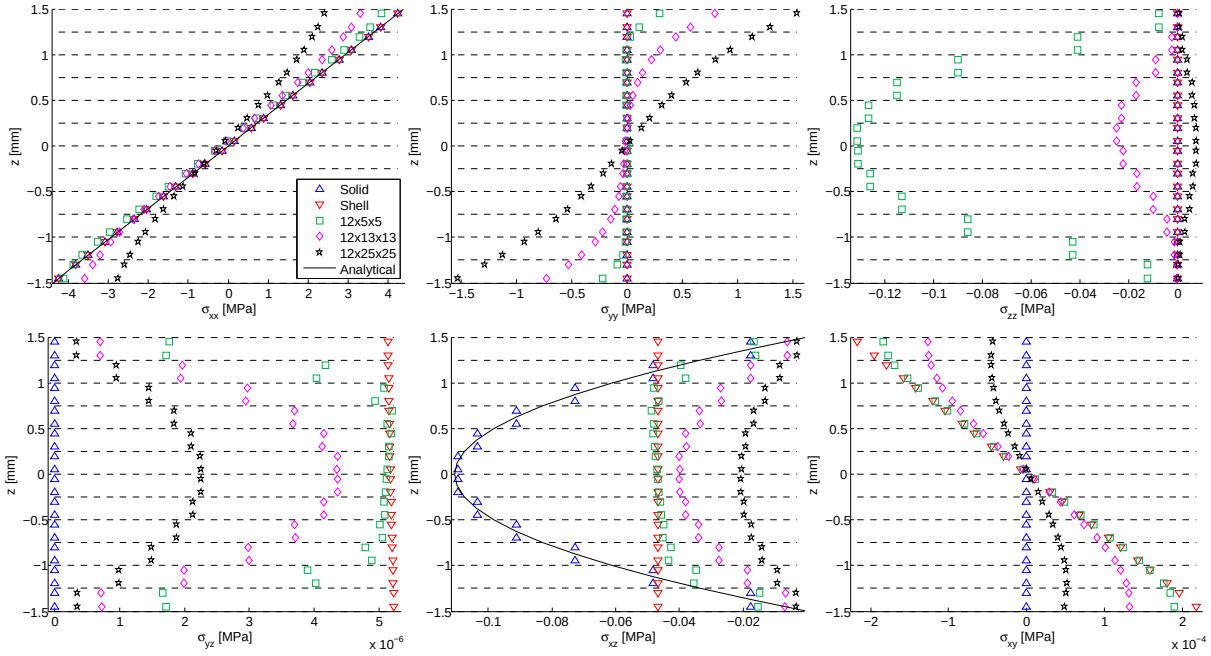

Figure 5. Stress components in the shell and solid models and three different RVE sizes for isotropic material.

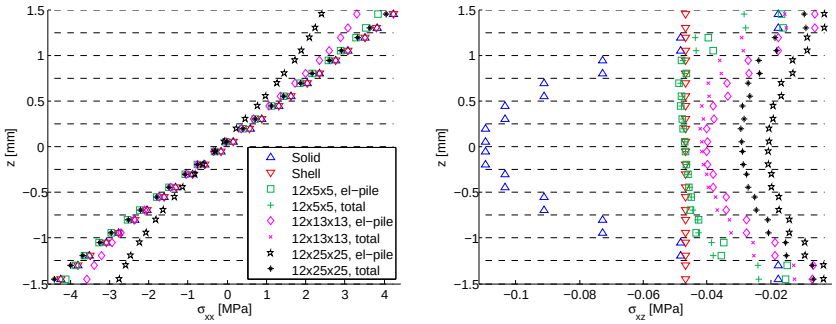

Figure 6. The in-plane integration point average for one element pile and the total elemental layer, respectively, for different RVE sizes compared to the shell and solid models. In-plane normal and out-of-plane shear stress components.

5. Conclusions

In this contribution, the potential of using a fully coupled multiscale method for simulating the mechanical response of fibre reinforced thin-walled laminates based on shell theory has been assessed. Only Dirichlet and a combination of Dirichlet and Neumann boundary conditions have been considered for the RVE. In the case of an isotropic plate, the results show that for the current multiscale approach, the size of the RVE cannot be chosen too large. If it is indeed chosen too large, the deformation mode of the RVE does not correspond to the one in the shell on the macroscale problem. This can partly be explained by the fact that the macroscale is determined by the laminate thickness, and the assumption that the averaged deformation field varies slowly enough within the RVE cannot be guaranteed at these RVE dimensions. It is clear that with the adopted boundary conditions, the 'best' results (in terms of stress distribution compared to the reference case in 3D) that can be achieved corresponds to what is obtained in the shell analysis. To accomplish results closer to the reference case with the given method, higher order expansion of the relative placement would probably be necessary. In the anisotropic case (transverserly

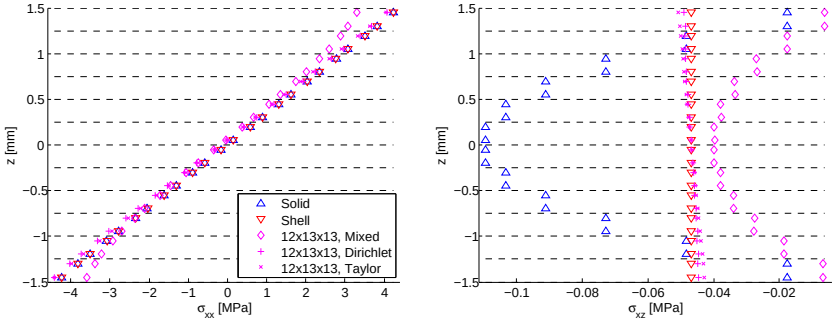

Figure 7. Effect of boundary condition type on the RVE in-plane normal and out-of-plane shear stress components.

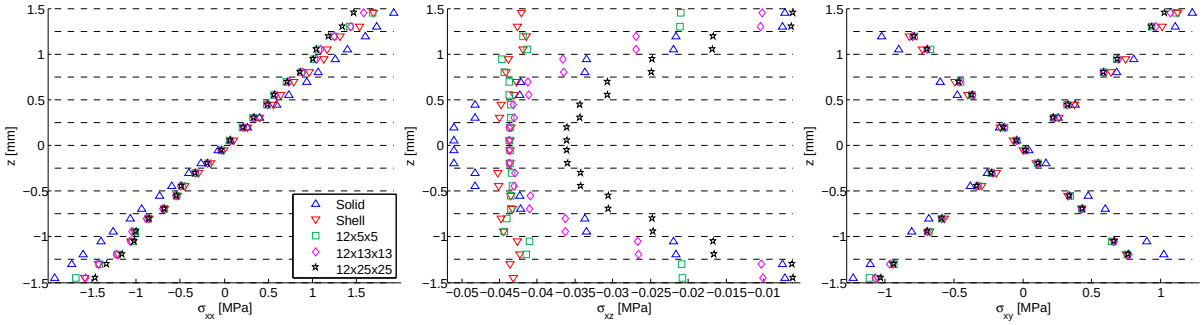

Figure 8. Relevant stress components in RVE:s of different sizes compared to the shell and solid models when orthotropic material is applied.

isotropic laminae), similar conclusions can be drawn. Noteworthy is however, that even if the in-plane normal stresses for the multiscale approach show a tendency for a somewhat larger deviation from the reference case (3D), the through-thickness shear stress variation is improved. We note that the potential of the proposed approach seems a bit limited in the case of homogeneous in-plane properties, but we believe that it would increase if one would investigate *e.g.* variations in the plane of the laminate in terms of voids or other geometrical imperfections.

References

[1] R. Larsson and M. Landervik. A stress-resultant shell theory based on multiscale homogenization. *Computer Methods in Appplied Mechanics and Engineering*, 263:1–11, 2013.

[2] V. Kouznetsova, M.G.D. Geers, and W.A.A. Brekelmans. Multi-scale constitutive modelling of heterogeneous materials with a gradient-enhanced computational homogenization scheme. *International Journal for Numerical Methods in Engineering*, 54:1235–1260, 2002.

[3] S. Hosseini, J.J.C. Remmers, C.V. Verhoosel, and R. de Borst. An isogeometric continuum shell element for non-linear analysis. *Computer Methods in Applied Mechanics and Engineering*, 271:1–22, 2013.

[4] E.W.C. Coenen, V.G. Kouznetsova, and M.G.D. Geers. Computational homogenization for heterogeneous thin sheets. *International Journal for Numerical Methods in Engineering*, 83:1180–1205, 2010.